
Modelling inorganic solids and their interfaces: A combined approach of atomistic and electronic structure simulation techniques

Stephen C. Parker,^a Sebastien Kerisit,^a Arnaud Marmier,^a Sonja Grigoleit^b and Graeme W. Watson^b

^a *Department of Chemistry, University of Bath, Claverton Down, Bath, UK BA2 7AY. E-mail: s.c.parker@bath.ac.uk; Fax: +44 1225 386231, Tel: +44 1225 386505*

^b *Department of Chemistry, Trinity College, Dublin 2, Ireland. Tel: +353 1 608 1357*

*Received 3rd December 2002, Accepted 16th January 2003
First published as an Advance Article on the web 14th May 2003*

We are seeking to combine the reliability of the structures and energies obtained from quantum mechanical methods with the insights given by larger scale simulations, which are better able to search configurational space. We will discuss our recent work using quantum mechanical methods, based on DFT, which have been applied to the study of a number of solids, Al₂O₃, CeO₂, MnO₂ and CaCO₃, and compare these with results using atomistic simulation where the forces between atoms are modelled using interatomic potentials. The results show that such quantum methods can be used successfully to screen the different potential models and where necessary, provide sufficient data to allow us to re-consider the potential models. In addition, we show examples where the quantum based methods can give further insights into the reactivity, particularly of surfaces. However, it still remains computationally expensive to search all possible configurations and by using the atomistic simulations to search through different configurations we can identify new structures which can be verified with the quantum based simulations.

Introduction

The aim of this paper is to describe our current work using a range of simulation techniques to model the structures and energetics of inorganic solids, with particular emphasis on the surfaces and interfaces of oxides and minerals. Interfaces control many of the important physical and chemical properties and hence deriving a detailed description of interface structure and its reactivity is central to improving our understanding for many fields, not least the study of crystal growth, chemical sensing, catalysis, remediation and corrosion.¹⁻⁴ However, experimental studies capable of determining the stability for a given interface structure, particularly for polar solids, are difficult and thus simulation provides a useful complementary technique for probing interfaces at the atomic level.

A central requirement for predicting key physical properties quantitatively is that the forces and the interaction energies between the atoms need to be described accurately. It is now possible to

achieve a high level of reliability for condensed phase materials with the use of quantum mechanical techniques based on density functional theory.⁵ Thus it is no surprise that there has been considerable work in this area and that many oxides and minerals have been studied using this approach, particularly using pseudopotentials for the core electrons to reduce the computational cost.⁶ The major limitation of the available DFT codes for routine use is still the high computational cost. This is particularly acute for studying the surface structure and energy of an oxide or mineral as each surface cut may have more than one low energy termination, the surface may be non-stoichiometric or even charged. Depending on the property studied each of these may have to be considered before investigating the effect of the impurities. Therefore the simulation of a single surface may require many tens of simulations for a simple oxide to many hundreds for a complex mineral.

Our approach for overcoming the problem of computational cost is to use atomistic simulation techniques to complement the quantum mechanical simulations. Atomistic simulations differ in that the forces between the atoms are specified by parameterised analytical equations, called a potential model, and hence the forces can be evaluated rapidly. The limitation is that the parameterisation can not be assumed to be perfect and thus the results from such simulations must be checked against quantum mechanical calculations and experimental data not used in the original parameterisation. If there are no suitable potentials available we can use the quantum simulations to help derive the parameters for the model. The atomistic simulations can then be used to perform a search of configurational space to identify other likely structures worthy of study using the electronic structure methods. The electronic structure simulations are then extended to calculate properties not accessible to the atomistic models, such as electron density and oxygen chemical potential, but with the confidence that we have a sensible surface structure. The atomistic simulations are extended to simulate for example, the effect of temperature on a large system of atoms, with the increased confidence in the reliability of the forces.

The approach of using electronic structure and atomistic simulation approaches together is now becoming established.^{7–9} To date we have applied these complementary methods to study the oxide–metal interface, where for the MgO–Ag interface we tested potential models for the metal–oxide interaction¹⁰ and secondly, the interaction of CaO with water molecules¹¹ to give us more insight into the oxide–water interface. Another earlier example has been our attempts at modelling lead oxides.¹² The work was able to give useful insight about the electron density of lead oxide, but in this case it was not useful for developing simple interatomic potentials because the stereochemical lone pairs were not stereochemical in that they were not just dependent on the lead but also on the type and geometry of ligands. Thus no transferable potential could be derived without recourse to a more sophisticated model.

In this paper we will illustrate our use of these techniques by describing four examples that are currently under investigation. Although the work in each of the areas is ongoing and not complete, it does show different but related synergistic applications of atomistic and quantum simulations. Initially, we will describe work on CeO₂, important for its catalytic properties. The difficulty is that there are a large number of different potential models, many of which have been derived independently and each can show agreement with available experimental data, but they differ in their predictions of how the surfaces relax. The aim is thus to use reliable electronic structure simulations to resolve the controversy and identify the best potential for this and future studies. We next consider the defective layered manganese(IV) oxide, birnessite. The difficulty is that it cannot be synthesised as the pure stoichiometric structure, therefore before modelling the defective material we require insight into the stability of the stoichiometric end-member and its relationship with the most stable polymorphs of MnO₂, ramsdellite and pyrolusite. The third example is where we have begun to use the electronic structure calculations to consider water adsorption on carbonate, particularly calcium carbonate surfaces. Finally, following preliminary work on alumina surfaces,¹³ we use the electronic structure simulations to explore the change in stoichiometry with oxygen partial pressure following the approach suggested by Finnis and co-workers.¹⁴ However before discussing the results we will briefly summarise the simulation approach.

Theoretical methodology

Our approach for modelling surfaces and interfaces is to focus on the most common surfaces of a crystal. The most common surfaces are those with lowest surface energy and are generally those of

low Miller index. These planes are the closest packed with large interplanar spacings. However in ionic crystals other constraints also apply. If the Madelung sums are not to diverge with increasing crystal size then the crystal must not only be electrically neutral but also have no net dipole moment perpendicular to the surface. Bertaut¹⁵ demonstrated that when there is a dipole moment perpendicular to the surface, the surface energy diverges and is infinite. Such surfaces are therefore unstable, and cannot occur naturally without the adsorption of foreign atoms or surface roughening to quench the dipole.

The simulation strategy is first to cleave a crystal to generate a slab or block which is charge neutral and symmetric about a mid point in the block. The crystal faces fall into three categories. Type I surfaces are comprised of stoichiometric planes, common examples include the {100} and {110} surfaces of rock salt and have equal numbers of cations and anions. Thus cleaving between the layers will yield a non-dipolar repeat. Type II surfaces are where the crystal planes perpendicular to the surface are charged and hence require more care as these must be cut at a specific plane to produce a non-dipolar slab. Type III surfaces cannot be cut at specific plane to remove the dipole moment. In order to remove the dipole the surfaces must undergo substantial reconstruction. As a consequence they are often the least stable.

The final structure (and energy) of a surface is then determined by the requirement that the system is in mechanical equilibrium. This is achieved by allowing the ions in the surface region to relax to the point at which they experience zero force. The number of relaxed surface planes is increased to the point at which the surface energy converges. Defects and impurities can then be accommodated in the surface. To date, we have modelled systems where the net charge is zero.

The atomistic simulations are based on the Born model of ionic solids, in which the ions interact *via* long-range electrostatic forces and a short-range term which includes a shell-model description of the ions to account for electronic polarisation.¹⁶ However, for more complex materials, particularly those containing polyanions it is often necessary to include angle dependent terms to account for the covalency, as is the case for calcium carbonate.¹⁷

We used the computer code METADISE¹⁸ which follows the two-region method developed by Tasker¹⁹ to perform static calculation at 0 K. In this approach the surface is separated in two regions periodic in two dimensions: a near surface region where the ions are allowed to relax mechanically and a second region where the ions are held fixed at their equilibrium positions. The Parry technique²⁰ was employed to calculate the electrostatic forces while parameterised analytical functions describe the short-range interactions. To investigate the effect of temperature on the surfaces we used the molecular dynamics code DL_POLY.²¹

The quantum mechanical total energy and structure of the systems were determined using density functional theory with the computer program VASP (Vienna *ab initio* simulation package).²² VASP can employ ultra-soft 'Vanderbilt' pseudopotentials²³ developed further by Kresse²⁴ which allow a smaller basis set for a given accuracy. Within the pseudopotential approach only the valence electron are treated explicitly.

An alternative, and more expensive, approach is to use the projector-augmented wave (PAW) method²⁵ to remove the core electrons from the calculations. While in the pseudopotential approach the core wavefunctions are replaced by a smooth nodeless functions, the PAW method is a highly efficient all-electron implementation that takes advantage of a combined basis set consisting of plane waves and one-centre orbitals.

In both cases the calculations were performed within the generalised-gradient approximation (GGA), using the exchange–correlation potential developed by Perdew *et al.*²⁶ The optimisation of the atomic coordinates was performed *via* a conjugate-gradients technique, which utilises the total energy and the Hellmann–Feynman forces on the atoms. The systems were relaxed until the change in total energy was smaller than 10^{-5} eV. It is important that the total energies are well converged. In all calculations, we insured that the total energies were converged with respect to the plane-wave cut-off and the density of *k*-points.

The low index surfaces of CeO₂

Ceria is an important component in three-way catalysts for the treatment of automobile exhaust gases²⁷ owing to its ability to store and release oxygen during surface reactions. A key requirement in understanding this reactivity is to understand the surface structure.

Table 1 Relaxed surface energies of the low index surface of CeO₂; AS1: atomistic simulation using potential 1, AS2: atomistic simulations using potential 2, DFT: density functional theory

Surface	Surface energies/J m ⁻²		
	AS1	AS2	DFT
{111}	1.22	1.36	0.68
{110}	1.59	2.14	1.01
{100}	2.05	2.91	1.41

Atomistic simulations with a range of different potentials have been used previously to examine both the surface and bulk properties of CeO₂. Several of them have predicted the surface energies and structures of the low index surfaces {100}, {110} and {111}. We have investigated the quality of a range of available potentials by comparing, with density functional theory (DFT) calculations, the calculated surface energy and extent of surface relaxation. Here we present the results of two of them, potential 1, by Sayle *et al.*²⁸ and potential 2, by Vyas *et al.*²⁹ Table 1 shows the surface energies for the three low index surfaces. Qualitatively the results are in agreement with the surface energies in the order {111} < {110} < {100}. Quantitatively the DFT energies are significantly smaller than those obtained using atomistic simulation. The reason for the lower values appears to be the inclusion of electron correlation as Hartree–Fock calculations³⁰ give surface energies closer to the atomistic results.

Detailed comparison of the relaxation of the surfaces was made with the relaxation normal to the surface plotted for the {111} in Fig. 1. Positive values indicate that the ions relax out of the surface, whereas negative values indicate displacement into the bulk. The Ce shell in both potential models more closely follows the DFT Ce relaxation with the cores displaced in opposite directions. For the oxygen, potential 2 significantly overestimates the relaxation while again for potential 1 the shell more closely matches the DFT atom location. Similar results were obtained for the {110} and {100} surfaces.

Potential 1 reproduced the structure only if we consider the shell position to represent the atom location. In atomistic models it is usual for the shell to represent the electronic polarisation and so the location of the shell would not be expected to have any crystallographic significance. However this model has a positive cation shell charge and therefore it could be argued that the shell represents the cation position. The O shell has a negative charge and thus would be expected to polarise in the normal way and yet this still represents a location significantly closer to the O found using DFT.

Potential 2 has a negative Ce shell charge and thus the polarisation of the Ce at the surface is reversed (see Fig. 1) and the potential model takes on the normal interpretation of the shell model with the core being located where the atom would be expected. The oxygen only polarises slightly with significant overestimation of the surface relaxation compared to the DFT calculations.

The comparisons of the surface relaxation of the potential models highlights problems with the definition of the shell model parameters when predicting the structure of surfaces. Further work will look at deriving new potential models with more reasonable and accurate shell parameters to ensure that the structural predictions are accurate. Such parameterisation will draw on the DFT calculations for not only the structure but information regarding the polarisation of atoms at the surface. By utilising this information we hope to be able to model not only the structure but the response of the surface to defects, such as surface oxygen vacancies that are important in oxygen storage capacity and CeO₂ reactivity.

Manganese dioxide

The ultimate aim of this work is to model the surface structure and reactivity of the important layered mineral birnessite in contact with aqueous solution. Not only is it an important manganese mineral, it reacts with organic compounds in the soil³¹ but is also associated with remediation, for example it has been suggested as a means of lowering the concentration of dissolved As(III) in drinking water.³² The reactivity stems from the ability of the surface Mn(IV) to reduce to Mn(III).

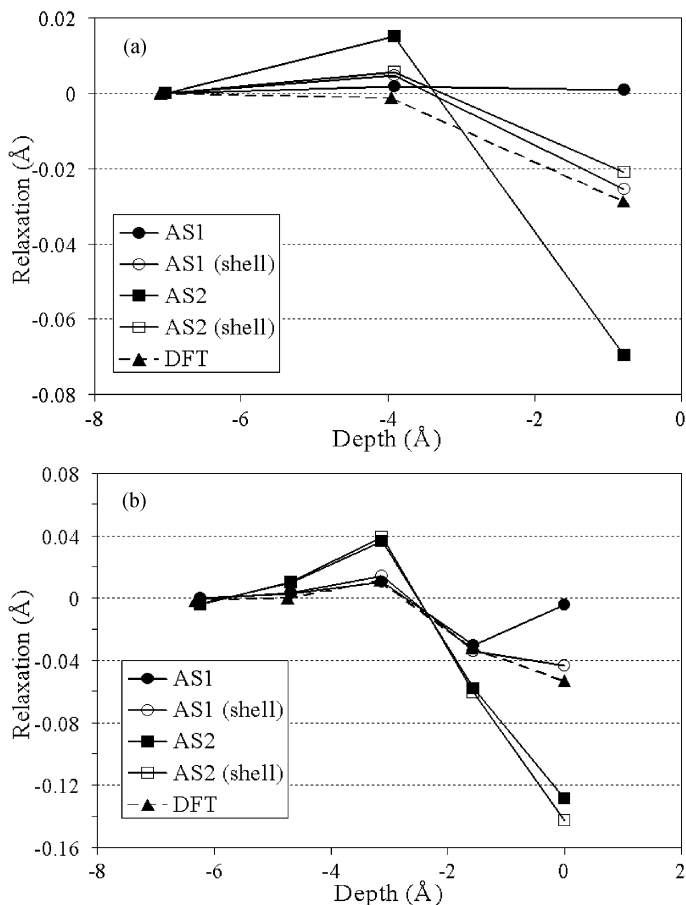


Fig. 1 Relaxation of (a) cerium and (b) oxygen at the (111) surface with respect to their bulk terminated positions as a function of depth. (AS n : atomistic simulation using potential n , shell: using shell location, DFT: density functional theory calculation).

The problem with modelling the mineral is that it is always highly defective and has not been observed as a pure phase. There is, therefore, insufficient experimental data to verify the simulations and to be sure that our simulations are considering the correct geometries we need to be able to consider a large number of configurations and the only way of obtaining detailed structural information of the end member is *via* electronic structure calculations. The treatment of pure MnO₂ is further complicated by the fact the two major phases pyrolusite and ramsdellite are themselves rarely observed in pure forms. Indeed the control of the phases is of interest to the battery industry as MnO₂ is widely used, and not unsurprisingly has been subject to recent theoretical investigation.^{33,34}

In this paper we summarise our initial work at modelling the layered manganese dioxide phase and its relationship to the other phases.

The birnessite structure is comprised of manganese octahedrally coordinated to oxygen. The octahedra are edge linked, forming MnO₂ sheets, Fig. 2a, and the oxygen ions are three coordinate but in a pyramidal geometry. This in contrast to the rutile-structured pyrolusite phase which has rows of edge linked octahedra, where each row is corner linked to its neighbour, Fig 2b. The cations are again linked to three coordinate oxygen ions but the three cation-oxygen bonds are in the same plane, *i.e.* the geometry of the oxygen bonding is more reminiscent of sp² hybridisation, rather than the sp³-like of birnessite. The second major phase, ramsdellite, has both types of

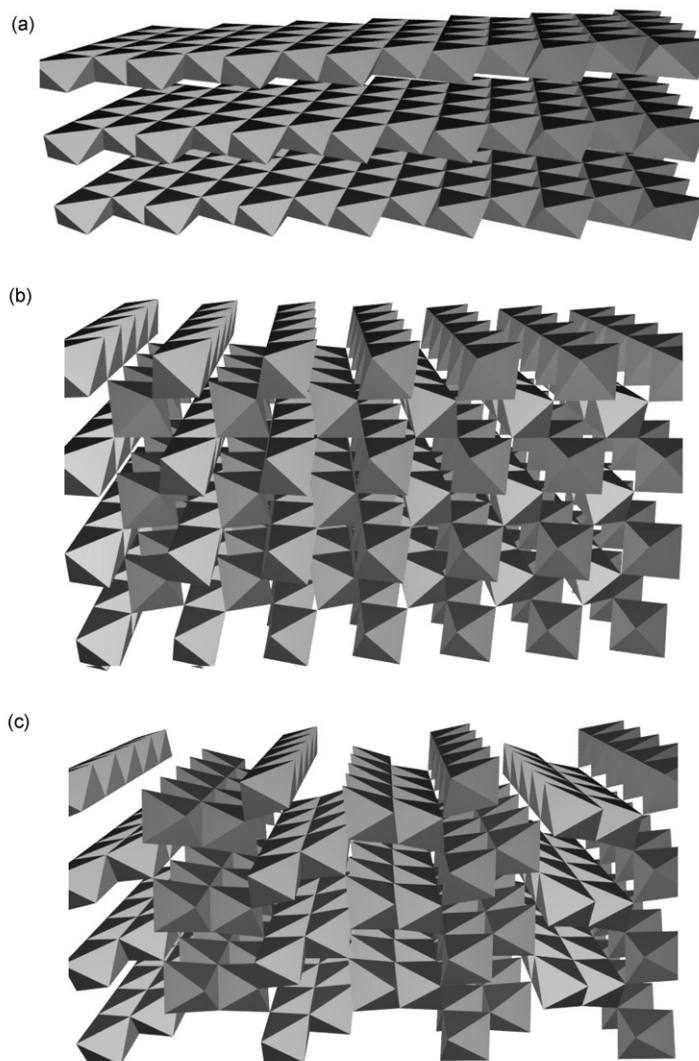


Fig. 2 The MnO_2 structures (a) AAAA birnessite, (b) ABAB pyrolusite and (c) AABB ramsdellite.

oxygen, and has double rows of edge linked octahedral, again these are corner linked to adjacent double rows, Fig. 2c. Examination of the structure shows that there are two cation sites, and by assigning the symbol A to one site and B to the other we can generate a simple Ising model-like representation of the structures. If only one of the positions is occupied then the layering occurs forming birnessite and can be designated AAAA. The rutile structured-pyrolusite is obtained by the alternating sequence ABAB and ramsdellite by AABB.

This simple representation also allows us to write down a simple Hamiltonian which includes the self-energy of each unit, E_a , J_{aa} the interaction between like units and J_{ab} the interaction between unlike units. Thus the energy of birnessite, AAAA, will be $4E_a - 4J_{aa}$, *i.e.* for a cell containing four cations, there will be four times the self energy, and each unit will interact only with a similar unit. In contrast, the energy of pyrolusite, ABAB will be $4E_a - 4J_{ab}$.

This approach of analysing the structural relationships and ordering in inorganic solids has been considered before, *e.g.* by Price *et al.* on magnesium silicates³⁵ where the interaction parameters were fitted to energies generated by atomistic simulations and by Heine and co-workers using fitted

Table 2 Relaxed energies of different polymorphs of MnO₂ using both DFT and atomistic simulations with the fitted interaction parameters

	Electronic structure		Atomistic
	E (per 4 Mn) no spin/eV	E (per 4 Mn) with spin/eV	Lattice energy (per 4 Mn)/eV
AAAA birnessite	-90.57	-95.71	-160.84
ABAB pyrolusite	-93.27	-96.06	-165.64
AABB ramsdellite	-92.44	-96.03	-163.34
Interaction parameters			
$2E_a$	44.19	44.81	79.32
J_{ab}	1.31	1.63	1.76
J_{aa}	0.63	1.55	0.56

DFT calculations for SiC polymorphs.³⁶ Although in both cases next nearest neighbour interaction energy parameters were also derived.

The energies for the three phases are calculated and given in Table 2, along with fitted interaction energy parameters. The results show that the energy differences are significantly reduced by allowing the simulation to include spin polarisation. Indeed, the energies of pyrolusite and ramsdellite become almost identical, not totally unexpected as both phases are usually present when synthesised. For comparison, Table 2 also gives the results from a rigid ion potential based on the model developed by Matsui and Akoagi for rutile.³⁷ The self-energy will be different because the standard state of the different calculations is different, but there are also large differences in the interaction energy parameters. The standard atomistic potential shows, not unlike the traditional Ising model, that there are large energy differences between the interaction of like and unlike units. However, by including the polarisability the interaction energy parameters become almost identical.

Simply to illustrate the scope of this approach, we next used these interaction energies to generate the energy of a large simulation cell, of 96 units and ran a Monte Carlo simulation where the geometry was varied randomly and the new structure was either accepted or rejected using the standard Metropolis algorithm at each temperature. Fig. 3 shows the concentration of the different sequences as a function of temperature. At low temperatures the pyrolusite is the dominant phase at low temperatures and becomes disordered at high temperatures. However, to complete the simulation we do need to consider a wider range of possible phases so that we can introduce next nearest neighbour interactions, and also investigate the effect of added impurities.

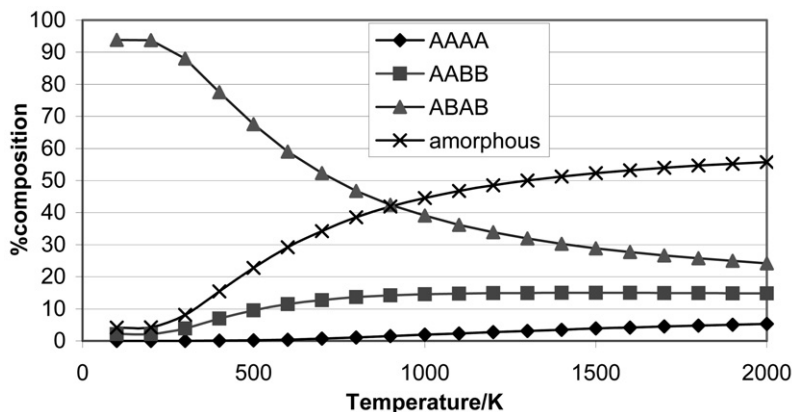


Fig. 3 Results from a Monte Carlo simulation indicating the relative concentrations of the three polymorphs and amount of disordered material.

Carbonate surfaces

Crystal growth of carbonate minerals is of major importance in both geological and biological systems. If we want to treat the growth process we would need to perform many large scale simulations. Atomistic simulation can achieve such system sizes but currently lacks the assured accuracy of the quantum mechanical approaches. Therefore the aim of this work is to investigate whether our currently favoured potential model agrees with electronic calculations for small model systems by comparing the calculated structure and energy of dry surfaces of calcite and the adsorption of water on the surfaces of different carbonates.

Dry slabs of four low index surfaces of calcite, the $\{10\bar{1}4\}$, $\{0001\}$, $\{10\bar{1}1\}$ and $\{11\bar{2}0\}$ with the $\{0001\}$ surface terminated in two different ways, either by a layer of calcium atoms or by carbonate groups were simulated using both DFT and atomistic simulation utilising the potential model derived by Pavese *et al.*¹⁷ for calcite. Table 3 compares the surface energies of the relaxed dry surfaces obtained from the potential model and DFT as well as the order of stability relative to the $\{10\bar{1}4\}$ surface.

It is clear from Table 3 that the potential model overestimates the surface energy of all the surfaces because of its lack of full electronic relaxation. Both models find the $\{10\bar{1}4\}$ to be the most stable surface and the $\{11\bar{2}0\}$ surface the least stable surface. Moreover, they agree on the relative stability of the different surfaces except for the $\{10\bar{1}0\}$ surface, which is more stable in the electronic structure calculations relative to the other surfaces. It is also worth noting that, although very small, the difference in surface energy between the calcium and carbonate terminated surface is the same for both approaches. By comparing the relaxation of all the surfaces obtained from the two types of calculations, we find that the carbonate molecule is more flexible in the electronic structure calculations. For example, such calculations predict that the carbon–oxygen bond distances range from 1.29 to 1.37 Å while in the potential model the bond distance is either 1.19 or 1.20 Å. Also, oxygen–carbon–oxygen bond angles calculated by the two approaches differ by less than 3° and the carbonate torsion angles are within 0.5° except for a few instances where the difference is up to 3°. These results support our view that both our bending and torsion angle potentials are satisfactory but that the parameters for the carbon–oxygen Morse potential need to be modified to improve agreement.

Table 3 also shows the surface energy of the calcite surfaces obtained from dynamic calculations using the potential model. Static and dynamic calculations agree on all the surface energies except one, namely the $\{11\bar{2}0\}$ surface. The configurations obtained from the two methods are shown in Fig. 4 and Fig. 5, where from Fig. 4 to Fig. 5 a surface carbonate group has rotated about its lattice site at the surface. An energy minimisation of the structure obtained from the dynamic calculation gives a lower surface energy, of 1.03 J m^{-2} using the potential model and 0.69 J m^{-2} from the electronic structure calculation. These calculations suggest that, to avoid being trapped in local minima, the surfaces of molecular ionic minerals, where rotation of the molecular species can occur, should be treated dynamically. As a molecular dynamics electronic structure calculation of each surface would require a large amount of computer time, we suggest an efficient alternative would be to use atomistic simulations to first perform a configuration search and then use the electronic structure based simulations to obtain accurate surface energies.

Table 3 Surface energies in J m^{-2} of the relaxed calcite surfaces as obtained from the two models

Surface	Atomistic simulation			Electronic structure	
	Static		Dynamic	Static	
	Relaxed	$\gamma_{\{10\bar{1}4\}}/\gamma$	Relaxed	Relaxed	$\gamma_{\{10\bar{1}4\}}/\gamma$
$\{10\bar{1}4\}$	0.59	1	0.52	0.42	1
$\{10\bar{1}0\}$	0.95	0.62	0.87	0.58	0.72
$\{0001\}$ Ca	0.97	0.61	0.89	0.66	0.64
$\{0001\}$ CO ₃	0.60	0.60	0.91	0.68	0.62
$\{11\bar{2}0\}$ static	1.39	0.42	0.99	0.95	0.44
$\{11\bar{2}0\}$ dynamic	1.03	0.57	—	0.69	0.61

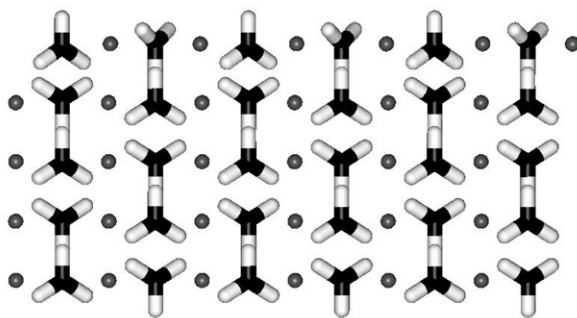


Fig. 4 The $\{11\bar{2}0\}$ surface as obtained from a static calculation with the potential model.

We are now extending this work to consider other carbonate minerals and compare their structures. For example, we have modelled the dry slabs of the $\{10\bar{1}4\}$ surfaces of calcite, dolomite and magnesite. The surface energies we obtained from the electronic structure calculations for the three minerals are very similar as shown in Table 4. The differences are very small and it seems that the surface energy increases slightly with the amount of magnesium in the crystal. In comparison, the potential model reproduces this trend but the differences in surface energy are much greater. We next adsorbed a monolayer of water onto the relaxed surfaces, with different starting configurations for the water molecules. We found two distinct adsorption geometries and used the relaxed position of the water molecules from the atomistic simulations as starting point for the electronic structure calculations. The results of the electronic structure calculations and atomistic simulations are shown in Table 5 for calcite and the relaxed structures in Fig. 6 and Fig. 7. For each mineral, the first mode of adsorption is energetically more favoured. The difference in surface energy between the two modes for each mineral is small and ranges from 0.06 to 0.15 J m⁻² while the difference in hydration energy varies from 7 to 16 kJ mol⁻¹. The atomistic model reproduces these differences: the surface energy difference varies from 0.10 to 0.13 J m⁻² and the hydration energy difference from 8 to 13 kJ mol⁻¹. Although the hydrated magnesite surface is calculated to be the most stable surface using both methods, the surface is stabilised to a greater extent by the presence of water in the atomistic simulation. In addition, the calculated magnesium–water oxygen distances using the potential model are shorter by as much as 0.3 Å. This may account for the fact that the hydration energy of the magnesite surfaces is much more exothermic, by about 35 kJ mol⁻¹, than estimated by the electronic structure calculations and that the surface energy is much smaller than the other hydrated surfaces. This is in contrast to the calcium–water oxygen distances which differ by less than 0.05 Å between the two models suggesting that the parameters for the calcium–water oxygen potential are satisfactory. Another major difference between the results of two methods is that in the potential model the water molecules preferentially form two long hydrogen bonds with the surface, whereas in the electronic structure calculations the water molecules form one short and one longer hydrogen bond. For example, in the case of calcite, the water hydrogen–carbonate oxygen

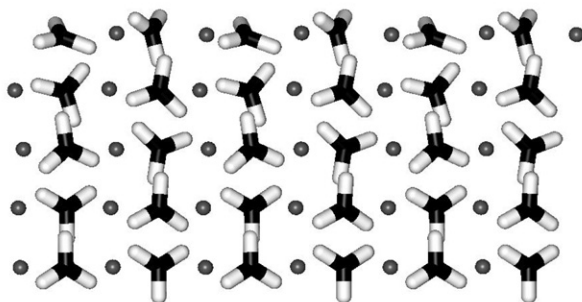


Fig. 5 The $\{11\bar{2}0\}$ surface as obtained from a dynamic calculation with the potential model.

Table 4 Surface energies/J m⁻² of the dry {1014} surfaces of calcite, dolomite and magnesite

Mineral	Atomistic simulation	Electronic structure
Calcite	0.59	0.426
Dolomite	0.64	0.437
Magnesite	0.76	0.464

distances for the first mode of adsorption of water are 1.66 and 2.42 Å in the DFT calculations and 1.97 and 2.05 Å in the atomistic simulations. This could explain the fact that the hydration energy of calcite as calculated by the potential model is more endothermic by about 20 kJ mol⁻¹.

In the light of these results, we ‘fine-tuned’ the magnesium–water oxygen and the water hydrogen–carbonate oxygen potentials to improve the agreement with the electronic structure calculations. Table 5 shows the results of the new potential under the column ‘potential model 2’. For each mineral the difference in energy between the two modes remains the same but the relative stability of the different hydrated mineral surfaces and the hydration energies are much closer to those obtained with the electronic structure calculations.

In conclusion, atomistic simulations helped to determine the preferred adsorption modes of water, of which the accurate structure and energetics could be calculated using density functional theory. This has enabled us to identify weaknesses in the potential model and to modify the relevant parameters to better reproduce the electronic structure calculations. The ultimate goal of this process is to be able to investigate large systems that would be too expensive to treat with a quantum mechanical model and still be confident that we are performing a high accuracy calculation. For example, in the future we want to investigate the free energy profile of atoms and molecules approaching the surface from the bulk of an aqueous solution to try and understand the process of crystal growth.

Surfaces of alumina

In recent years the study of the surfaces of α -alumina by atomistic methods has been focused on the basal (0001) surface and on trying to elucidate its controversial relaxation, either experimentally^{38–42} or computationally.^{14,43–47} The energetics of other surfaces has been investigated by semi-empirical modelling¹³ and by DFT in its LDA approximation,⁴⁸ and has been restricted to stoichiometric terminations. Recent developments allow a new analysis to be carried, using the more modern GGA approximation and taking into account the oxygen partial pressure.^{14,15}

Consider an oxide of chemical formula A_mO_n , in chemical equilibrium with an O₂ vapour. This is modelled here as a slab of area S containing N_A metal atoms at chemical potential μ_A° and N_O oxygen atoms at chemical potential μ_O° .

Let us first define the excess in oxygen, as in ref. 49.

$$\Gamma_O = [N_O/N_A] = \frac{1}{2S} \left(N_O - \frac{n}{m} N_A \right). \quad (1)$$

Table 5 Surface and hydration energies of the hydrated {1014} surfaces of calcite, dolomite and magnesite

Mineral	Potential model 1		Potential model 2		Electronic structure	
	$\gamma/J\ m^{-2}$	$E_{\text{hydration}}/kJ\ mol^{-1}$	$\gamma/J\ m^{-2}$	$E_{\text{hydration}}/kJ\ mol^{-1}$	$\gamma/J\ m^{-2}$	$E_{\text{hydration}}/kJ\ mol^{-1}$
Calcite mode 1	0.34	-73.5	0.21	-88.0	0.04	-92.3
Calcite mode 2	0.44	-61.5	0.30	-77.9	0.10	-85.3
Dolomite mode 1	0.17	-94.6	0.25	-85.9	0.05	-88.7
Dolomite mode 2	0.27	-83.5	0.35	-74.8	0.12	-80.6
Magnesite mode 1	-0.10	-127.2	0.24	-94.3	-0.006	-93.6
Magnesite mode 2	0.03	-114.4	0.35	-83.7	0.15	-76.8

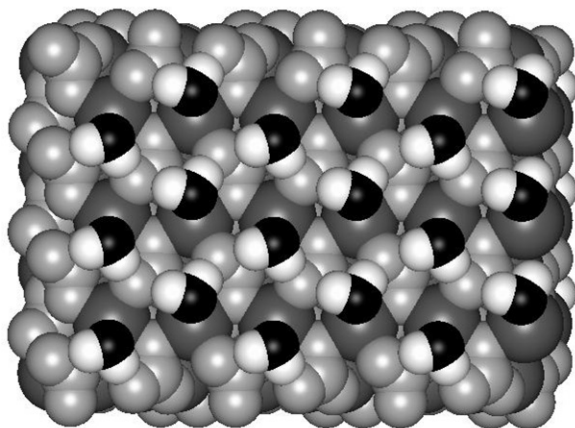


Fig. 6 Relaxed structure of the first adsorption mode of water from electronic structure calculation.

The surface energy is (as there are two interfaces due to the slab nature of the system)

$$\gamma_{\text{AO}} = \frac{1}{2S} (G_{\text{AO}}^{\text{slab}} - N_{\text{A}}\mu_{\text{A}} - N_{\text{O}}\mu_{\text{O}}). \quad (2)$$

The Gibbs energy per formula unit g_{AO} is related to the energy of the bulk but also to the chemical potential of A and O,

$$g_{\text{AO}} = \frac{m}{N_{\text{A}}} G_{\text{AO}}^{\text{bulk}} \quad \text{and} \quad g_{\text{AO}} = m\mu_{\text{A}} + n\mu_{\text{O}}. \quad (3)$$

By recombining, we obtain first

$$\gamma_{\text{AO}} = \frac{1}{2S} \left(G_{\text{AO}}^{\text{slab}} - \frac{N_{\text{A}}}{m} g_{\text{AO}} \right) - \Gamma_{\text{O}}\mu_{\text{O}}. \quad (4)$$

In this last equation, all the quantities can be extracted directly from *ab initio* calculations, with the exception of μ_{O} .

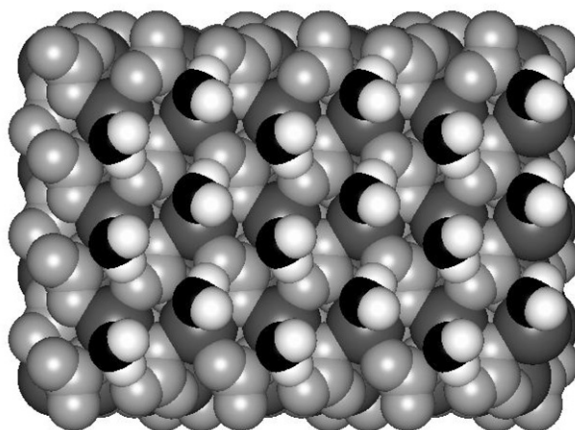
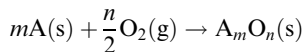


Fig. 7 Relaxed structure of the second adsorption mode of water from electronic structure calculation.

To access this last quantity, we invoke the standard ideal gas expression for the chemical potential of O in equilibrium with its vapour

$$\mu_{\text{O}} = \mu_{\text{O}}^{\circ} + \frac{1}{2}kT \log\left(\frac{P_{\text{O}_2}}{P^{\circ}}\right). \quad (5)$$

Calculating the energy of molecular oxygen presents difficulties for DFT, so we have to resort to using experimental quantities and a thermodynamic cycle. The standard energy of formation of the oxide, corresponding to the following equation,



is

$$\Delta G_{\text{f}}^{\circ}(\text{A}_m\text{O}_n) = g_{\text{AO}}^{\circ} - m\mu_{\text{A}}^{\circ} - n\mu_{\text{O}}^{\circ}, \quad (6)$$

from which it is straightforward to extract μ_{O}° as a function of μ_{A}° and g_{AO}° . The values for μ_{A}° and g_{AO}° can be extrapolated from 0K calculations (solid A and solid A_mO_n), and $\Delta G_{\text{f}}^{\circ}(\text{A}_m\text{O}_n)$ which has a tabulated experimental value of $-376.77 \text{ kcal.mol}^{-1}$ for α -alumina.⁵⁰ A note of caution here, as g_{AO}° depends on the pseudopotential used for the calculation, μ_{O}° must be computed using the same pseudopotential.

Inserting eqn. (6) into eqn. (4), we reach a workable expression for the surface energy

$$\begin{aligned} \gamma_{\text{AO}} = & \frac{1}{2S} \left(G_{\text{AO}}^{\text{slab}} - \frac{N_{\text{A}}}{m} g_{\text{AO}} \right) \\ & - \Gamma_{\text{O}} \frac{g_{\text{AO}}^{\circ} - m\mu_{\text{A}}^{\circ} - \Delta G_{\text{f}}^{\circ}(\text{A}_m\text{O}_n)}{n} \\ & - \Gamma_{\text{O}} \frac{kT}{2} \log\left(\frac{P_{\text{O}_2}}{P^{\circ}}\right). \end{aligned} \quad (7)$$

The first term in the rhs of eqn. (7) is the stoichiometric contribution to the surface energy, the second is the contribution of the excess oxygen at a pressure of P° (1 bar) and the last term is the temperature and pressure dependent component.

A last approximation consists of replacing the standard value g_{AO}° and μ_{A}° by their value at 0 K, g_{AO} and μ_{A} (possible because they are solids).

DFT-GGA calculations were performed on different surfaces/terminations of α -alumina (Fig. 8). We present in Fig. 9 two sets of results. First we pay special attention to the {0001} surface by considering the stoichiometric Al termination, the hypostoichiometric Al_2 termination, the hyperstoichiometric O_3 termination and a hydroxylated configuration of the later, O_3H_3 . Then we compare the relative stability of three surfaces, {0001}, {01 $\bar{1}$ 2} and {10 $\bar{1}$ 0}, chosen because they were those with the lower surface energy in the early LDA work.⁴⁸

There is currently a disagreement between theoretical and experimental description of the {0001} surface of alumina. Most studies find that in the absence of water the Al terminated surface is the most stable, and we will assume in the following discussion that this is the case. This surface experiences a strong relaxation, which is interpreted as the fact that the Al atoms sink into the plane of O atoms, but while experimental probes estimate the Al–O interplanar distance at roughly half its bulk value, *ab initio* (mostly DFT, but also HF) find an even more important relaxation where the Al–O interplanar distance is only 20% of the bulk value. To date, the different explanations to this puzzling behaviour, involving either localised anisotropic vibrational modes or adsorption of O or H at the surface have not been sufficient to explain the differences. No localised anisotropic very intense mode has been found yet and the changes of relaxation with adsorbate only marginally improves the agreement with experiment.

We consider the simple single species termination and ideal planar cleavage surfaces, {0001} Al, {0001} Al_2 and {0001} O_3 , as well as a H passivated, oxygen terminated surface, {0001} O_3H_3 .

None of these terminations compare especially well to the experimental relaxations, as can be seen in Table 6.

The closest is {0001} Al, which is also the one with the lowest surface energy under a reasonable range of oxygen partial pressure (see Table 7 and Fig. 9).

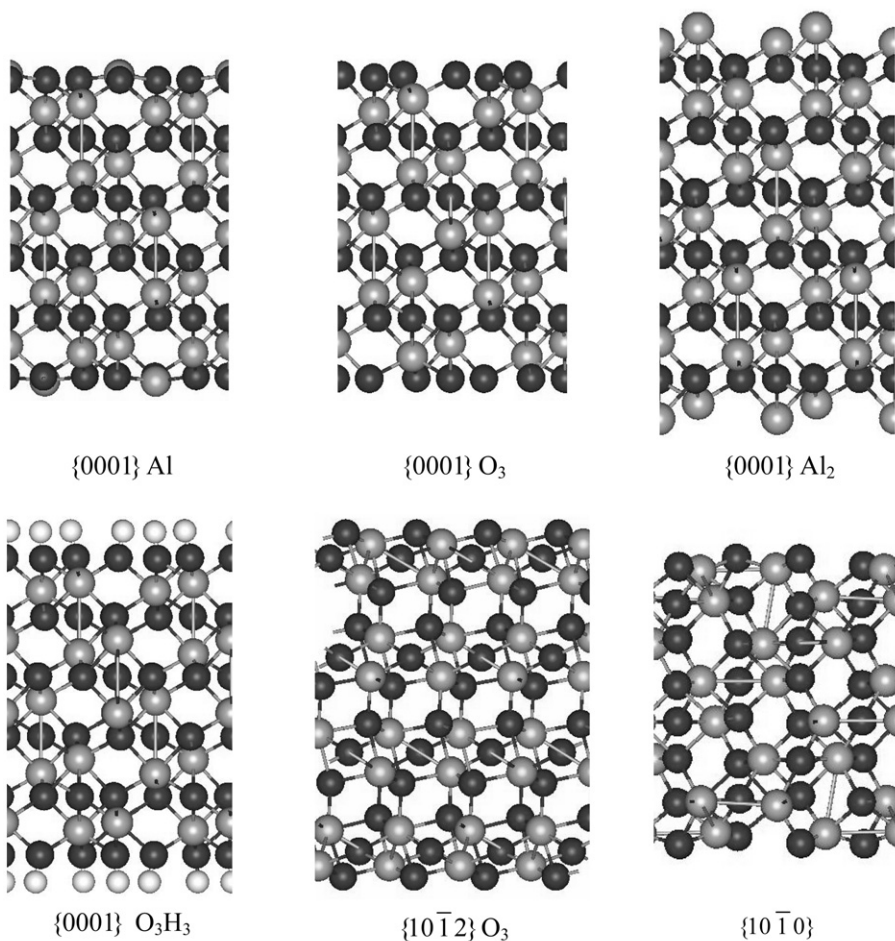


Fig. 8 Surfaces considered in this work.

The surface could reconstruct in a number of alternative structures, some of which have been investigated in ref. 42 but we do not believe that any of these will either match the experimental relaxations better or have a lower surface energy than $\{0001\}$ Al.

Our aim is ultimately to predict the morphology of the crystal, using a similar approach as described in ref. 13 but using *ab initio* modelling. We therefore need to compare the surface energy of different surfaces, for a range of temperatures and compositions.

Table 6 Relaxations for different terminations of the $\{0001\}$ surface

Surface	Al ₀ Al ₁	Al ₁ O ₁	O ₁ Al ₂	Al ₂ Al ₃	Al ₃ O ₂	O ₂ Al ₄
$\{0001\}$ Al	—	−80.1%	3.9%	−45.0%	19.7%	5.0%
$\{0001\}$ Al ₂	−41.4%	32.3%	1.3%	−4.1%	1.5%	0.1%
$\{0001\}$ O ₃ ^(a)	—	—	−2.7%	0.6%	3.6%	−0.6%
$\{0001\}$ O ₃ H ₃ ^(a)	—	—	6.0%	−39.1%	11.9%	−0.6%
Technique	First	Second	Third	Fourth		
X-ray ⁴⁰	−51%	16%	−29%	20%		
Tensor-LEED ⁴²	−50%	6%	—	—		

Table 7 Surface energy/J m⁻² of α -alumina surfaces

Surface	GGA, this work	LDA ⁴⁸	Shell ¹³
{0001} Al	1.94	1.76	2.42
{0001} Al ₂	9.60	—	—
{0001} O ₃	5.02	—	3.83 ^a
{1012}	2.02	1.97	2.385 ^b
{1010}	2.56	1.40	2.867 ^b

^a Represent a different surface, stoichiometric, with 0.5 of the O site occupied. ^b Recalculated using the same potential.

We present here very preliminary results where only the oxygen present in the vapour in equilibrium with the crystal is considered.

In Table 7, we show the calculated surface energies, as well as those previously obtained by DFT-LDA and atomistic modelling based on the shell model.

It is at first surprising that the new GGA results seem more in line with the atomistic simulations than with the LDA calculations. But the {10 $\bar{1}$ 0} requires a large cell, and therefore more computational power than was available in 1994 to simulate a sufficiently thick slab, and as noted by the authors of the original paper, the LDA value for this surface could not be relied on.

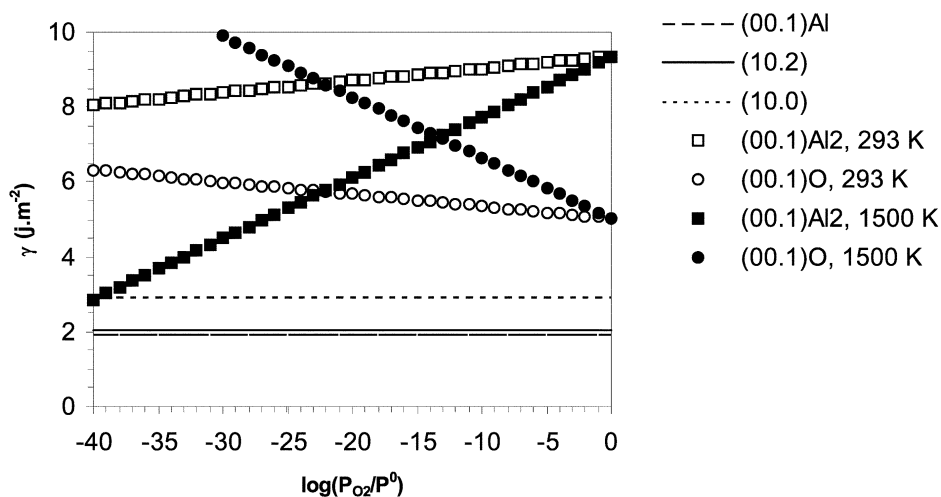
Conclusion

This study has shown the application of both DFT and atomistic simulation techniques to a number of inorganic solids.

The limitation of available computational resources means that for us the most effective means of modelling complex interfaces in inorganic solids is *via* atomistic simulation. However, the electronic structure simulation techniques do play a crucial role.

First of all, thanks to their superior accuracy, they provide a useful set of tools for screening, calibrating and developing interatomic potentials.

(i) In many cases there are different sets of parameters that can be used to model the same material. Hence a reliable approach for deciding which potential is best suited to the problem under consideration is valuable. Especially for interfaces, where we find that different potential models which can reproduce the same bulk behaviour, as for CeO₂, do show distinctly different surface



relaxations and hence even a moderately reliable electronic structure based simulation should be able to distinguish between them.

(ii) Another use of the quantum simulations is to obtain structural and thermodynamic data for these phases that cannot readily be synthesized experimentally, or to complete the set of experimental data for little studied materials.

Secondly, when the emphasis is more on the electronic structure calculations, one can use the advantages of the interatomic models in terms of speed and spatial scaling.

(iii) In the case of adsorption at complex surfaces, atomistic simulation methods are valuable for providing a preliminary search of the configurational space and quantitative criteria to pre-sort the different structures and hence reduce the amount of quantum calculation to be performed or increasing their scope. In our studies of calcite surfaces, several structural rearrangements, which had originally been missed by direct geometry optimization (DFT) of the bulk terminated surfaces, were discovered by using shell models.

(iv) Another use for interatomic models is to estimate the effect of some parameters which are typically used in quantum-mechanical simulations, without incurring the large cpu overheads. For example, using classical molecular dynamics to check the effect of temperature on a system is now standard practice, but one can also evaluate size effects, vibrational *k*-points sampling, harmonic versus quasi-harmonic approximation, disorder, interface with liquid and many others.

Finally, there are some phenomena that are very difficult to approach directly with simple potentials, such as the change of stoichiometry in alumina surfaces. In such cases, it is actually conceptually much simpler and cost effective to use directly an *ab initio* technique instead of expanding (possibly beyond a reasonable scope) an interatomic model.

In summary, DFT and atomistic simulation techniques show useful synergy when modeling structure, stability and reactivity inorganic oxides and minerals, the accuracy of the first complementing well the realism of the second, and together they form a useful complement to experiments.

Acknowledgements

We would like to acknowledge funding from EPSRC GR/H0413, GR/H0185, NERC/T/S/2001/00855, JREI award JR99BAPAEQ.

References

- 1 G. E. Brown, V. E. Herich, W. H. Casey, D. L. Clark, C. Eggleston, A. Felmy, D. W. Goodman, M. Gratzel, G. Maciel, M. I. McCarthy, K. H. Neelson, D. A. Sverjensky, M. F. Toney and J. M. Zachara, *Chem. Rev.*, 1999, **99**, 77.
- 2 M. G. Nooney, T. S. Murrell, J. C. Cornville, D. A. Wood and D. W. Goodman, *AVS 42nd National Symposium*, American Vacuum Society, 1995, p. 235.
- 3 ed. P. Marcus, J. Oudar, *Corrosion Mechanisms in Theory and Practice*, Marcel Dekker Inc., New York, 1995.
- 4 B. B. Rao, *Mater. Chem. Phys.*, 2000, **64**, 62.
- 5 M. C. Payne, M. P. Teter, D. C. Allan, T. A. Arias and J. D. Joannopoulos, *Rev. Mod. Phys.*, 1991, **64**, 1045.
- 6 P. J. D. Lindan, M. J. Gillan and N. M. Harrison, *Phys. Rev. Lett.*, 1998, **80**, 762.
- 7 D. Alfè, M. J. Gillan, L. Vocadlo, J. Brodholt and G. D. Price, *Philos. Trans. R. Soc. London, Ser. A*, 2002, **360**, 1227.
- 8 J. S. Braithwaite, C. R. A. Catlow, J. H. Harding and J. D. Gale, *Phys. Chem. Chem. Phys.*, 2001, **3**, 4052.
- 9 A. Aguado, L. Bernasconi and P. A. Madden, *Chem. Phys. Lett.*, 2002, **356**, 437.
- 10 J. A. Purton, D. M. Bird, S. C. Parker and D. W. Bullett, *J. Chem. Phys.*, 1999, **110**, 8090.
- 11 N. H. De Leeuw, J. A. Purton, S. C. Parker, G. W. Watson and G. Kresse, *Surf. Sci.*, 2000, **452**, 9.
- 12 G. W. Watson and S. C. Parker, *J. Phys. Chem. B*, 1999, **103**, 1258.
- 13 N. H. de Leeuw and S. C. Parker, *J. Am. Ceram. Soc.*, 1999, **82**, 3209.
- 14 I. G. Batirev, A. Alavi and M. W. Finnis, *Phys. Rev. B*, 2000, **62**, 4698.
- 15 F. Bertaut, *C. R.*, 1958, **246**, 3447.
- 16 B. G. Dick and A. W. Overhauser, *Phys. Rev.*, 1958, **112**, 90.
- 17 A. Pavese, M. Catti, S. C. Parker and A. Wall, *Phys. Chem. Miner.*, 1996, **23**, 89.
- 18 G. W. Watson, E. T. Kelsey, N. H. de Leeuw, D. J. Harris and S. C. Parker, *J. Chem. Soc., Faraday Trans.*, 1996, **92**(3), 433.

- 19 P. W. Tasker, *Philos. Mag. A*, 1979, **39**, 119.
- 20 D. E. Parry, *Surf. Sci.*, 1975, **49**, 433; D. E. Parry, *Surf. Sci.*, 1976, **54**, 195.
- 21 T. R. Forester and W. Smith, *DL_POLY user manual*, CCLRC, Daresbury Laboratory, Daresbury, UK, 1995.
- 22 G. Kresse and J. Hafner, *Phys. Rev. B*, 1993, **47**, 558; G. Kresse and J. Hafner, *Phys. Rev. B*, 1994, **49**, 14251; G. Kresse and J. Furthmuller, *Compt. Mater. Sci.*, 1996, **6**, 15; G. Kresse and J. Furthmuller, *Phys. Rev. B*, 1996, **54**, 11 169.
- 23 D. Vanderbilt, *Phys. Rev. B*, 1990, **41**, 7892.
- 24 G. Kresse and J. Hafner, *J. Phys. Condens. Matter*, 1994, **6**, 8245.
- 25 P. E. Blöchl, *Phys. Rev. B*, 1994, **50**, 17953.
- 26 J. P. Perdew, J. A. Chevary, S. H. Vosko, K. A. Jackson, M. R. Pederson, D. J. Singh and C Fiolhas, *Phys. Rev. B*, 1992, **46**, 6671.
- 27 A. Trovarelli, *Catal. Rev. Sci. Eng.*, 1996, **38**, 439.
- 28 T. X. T. Sayle, S. C. Parker and C. R. A. Catlow, *Surf. Sci.*, 1994, **316**, 329.
- 29 S. Vyas, R. W. Grimes, D. H. Gay and A. L. Rohl, *J. Chem. Soc., Faraday Trans.*, 1998, **94**, 427.
- 30 S. Gennard, F. Cera and C. R. A. Catlow, *J. Phys. Chem. B*, 1999, **103**, 10 158.
- 31 D. Banerjee and H. W. Nesbitt, *Geochim. Cosmochim. Acta*, 2001, **65**, 1703.
- 32 B. A. Manning, S. E. Fendorf, B. Bostick and D. L. Suarez, *Environ. Sci. Technol.*, 2002, **36**, 976.
- 33 D. Balachandran, D. Morgan and G. Ceder, *J. Solid State Chem.*, 2002, **166**, 91.
- 34 M. Zhuang and J. W. Halley, *Phys. Rev. B*, 2001, **64**, 24413.
- 35 G. D. Price, S. C. Parker and J. Yeomans, *Acta Crystallogr., Sect. B*, 1985, **231**, B41.
- 36 C. Cheng, R. J. Needs and V. Heine, *J. Phys. C*, 1998, **21**, 1049.
- 37 M. Matsui and M. Akoagi, *Mol. Sim.*, 1991, **6**, 239.
- 38 J. Ahn and J. W. Rabalais, *Surf. Sci.*, 1997, **388**, 121.
- 39 T. Suzuki, S. Hishita, K. Oyoshi and R. Souda, *Surf. Sci.*, 1999, **437**, 289.
- 40 P. Guenard, G. Renaud, A. Barbier and M. Gautier-Soyer, *Surf. Rev. Lett.*, 1998, **5**, 321.
- 41 J. Toofan and P. R. Watson, *Surf. Sci.*, 1998, **401**, 162.
- 42 E. A. Soares, M. A. Van Hove, C. F. Walters and K. F. McCarthy, *Phys. Rev. B*, 2002, **65**, 195405.
- 43 R. Di Felice and J. E. Northrup, *Phys. Rev. B*, 1999, **60**, R16 287.
- 44 I. G. Batirev, A. Alavi, M. W. Finnis and T. Deutsch, *Phys. Rev. Lett.*, 1999, **82**, 1510.
- 45 X. G. Wang, A. Chaka and M. Scheffler, *Phys. Rev. Lett.*, 2000, **84**, 3650.
- 46 W. Zhang and J. R. Smith, *Phys. Rev. Lett.*, 2000, **85**, 3225.
- 47 A. Marmier and M. W. Finnis, *J. Phys. Condens. Matter*, 2002, **14**, 7797.
- 48 I. Manassis and M. J. Gillan, *J. Am. Ceram. Soc.*, 1994, **77**, 335.
- 49 J. W. Cahn, in *Interfacial Segregation*, ed. W. C. Johnson and J. M. Blakely, American Society for Metals, Metal Park, OH, 1977, pp. 3–23.
- 50 *CRC Handbook of Chemistry and Physics*, ed. D.R. Lide, CRC press, Boca Raton, FL, 78th edn., 1997.